AD-A185 965 J-ESTIMATION PROCEDURE BASED ON MOIRE INTERFEROMETRY 1/1
DATA(U) WASHINGTON UNIV SEATTLE DEPT OF MECHANICAL
ENGINEERING B S KANG ET AL AUG 87 UWA/DME/TR-87/58
UNCLASSIFIED N00014-85-K-0187 F/G 20/11 NL

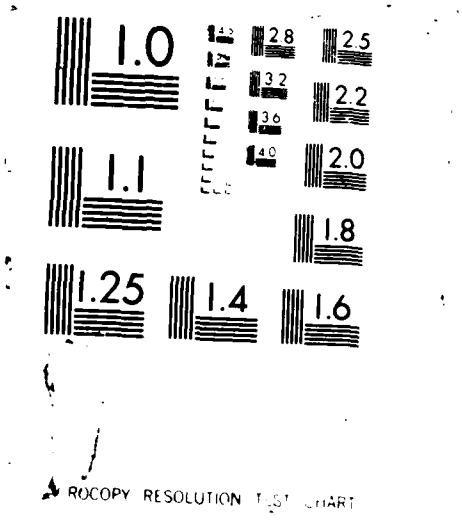
1.0
2.8
2.5
3.2
2.2
3.6
4.0
2.0
1.1
1.8
1.25
1.4
1.6
ROCOPY RESOLUTION TEST CHART

Office of Naval Research
Contract N00014-85-K-0187
Technical Report No. UWA/DME/TR-87/58

J-estimation Procedure based on Moire Interferometry Data

B.S.-J. Kang and A.S. Kobayashi

August 1987

The research reported in this technical report was made possible through support extended to the Department of Mechanical Engineering, University of Washington, by the Office of Naval Research under Contract N00014-85-K-0187. Reproduction in whole or in part is permitted for any purpose of the United States Government.

J-estimation Procedure Based on Moire Interferometry Data

B. S.-J. Kang and A. S. Kobayashi
University of Washington
Department of Mechanical Engineering
Seattle, Washington 98195

INTRODUCTION

The J-integral [1], which has been heralded by many as a stable crack growth and ductile fracture criteria and which in its linearly elastic limit becomes the strain energy release rate, derives its popularity in being a path-independent integral. Because of this path-independency, which is valid under the deformation theory of plasticity, the J-integral evaluated remotely is equal to that evaluated in the near vicinity of the crack tip and can thus be used to characterize the crack tip region. If the crack-tip state for a strain hardening of the Ramberg-Osgood power hardening type can be represented by the Hutchinson-Rice-Rosengren (HRR) field [2,3], then the J-integral becomes the amplitude of this singular stress field.

The path-independency of the J-integral has been exploited by the fracture mechanics community by evaluating the J-integral remotely, namely at the load-point of fracture specimens in numerous proposed and practiced test methods [4,5,6]. The J-integral also has been evaluated numerically along various contours inside the fracture specimen in the presence of both small and large scale yielding. The path-independency of the J-integral was preserved in the presence of a small crack extension of about 3 mm in moderately yielded A533B compact specimen [7]. The experimental counter-part of such studies, however, are missing due to the lack of an experimental procedure for evaluating the J-integral along contours within the specimen.

The purpose of this paper is to review an experimental procedure, which was developed by the authors [8,9], using moire interferometry, for estimating the J- integral values along contours inside fracture specimens and to present some resistance curves, R-curves, of aluminum single edge notched (SEN) specimens.

J-estimation Procedure

The J-estimation procedure consists of aprroximating the two dimensional states of stress and strain with the uniaxial states of stress and strains. For a SEN specimen shown in Figure 1, this replacement provides the exact states along the two lateral boundaries and crack faces. If the two horizontal paths in Figure 1 are sufficiently remote from the crack tip and if the SEN specimen is subjected to a simple loading, then this replacement also provides the exact states and thus the J evaluated along the most remote contour in

Figure 1 using the J-estimation procedure will yield the correct J-integral. Some of the mathematical expressions associated with the J-estimation procedure are listed in the following.

1. J-integral

For plane problems governed by nonlinear elaticity and deformation plasticity, the J-integral is defined as [1].

$$J = \int_{\partial} W\, dy - \vec{T} \cdot \frac{\partial \vec{u}}{\partial x} ds \tag{1}$$

where

Γ is the contour surrounding the crack tip

$\vec{T}$ is the traction vector along the contour

$\vec{u}$ is the displacement vector on the contour

W is the strain energy density on the contour.

When the above contour integral is applied to a single edge notched (SEN) specimen subjected to Mode I loading condition as shown in Fig. 1, only half of the coutour is needed from symmetry consideration. The integral value of Equation (1) along the traction-free vertical edges of segments 12 nad 34 in Fig. 1, is:

$$J_V = \int_{12+34} W\, dy$$

$$= (\Sigma W_i\, \Delta y_i)_{12} + (\Sigma W_i\, \Delta y_i)_{34} \tag{2}$$

where i is the ith segment of the contour.

If horizontal segment 23 is sufficiently far away from the crack, we can assume that the shear stress, τ_{xy}, and the x-direction variations in the displacement u_x are negligible along the segment 23. Equation (1) along segment 23 thus becomes:

$$J_h = \int_{23} T_y \cdot \frac{\partial u_y}{\partial x} dx$$

$$= \Sigma[(\sigma_{yy} \cdot \frac{\Delta u_y}{\Delta x})_i \Delta x_i]_{23} \tag{3}$$

Finally, the total J-integral value is given by:

$$J = 2(J_v + J_h) \tag{4}$$

The above J-evaluation procedure lends itself to determining the J-integral value experimentally by using strain gages and linear variable displacement transducers at discrete points along the specimen boundary [10-12]. Since the test data in these references were obtained from few locations along the specimen boundaries, Equation (4) could only be evaluated at isolated discrete locations. Continuous experimental data for the J-evaluation, on the other hand, can be obtained through the used of moire interferometry with better accuracy and requires only a single u_y-displacement moire field for calculating the J-integral.

Near-field J-integral Measurement

While the above procedure is valid for far-field J-integral evaluation, its validity for the near field integration contour, such as the inside rectangular contour shown in Fig. 1, must be justified. Reference [8] showed that for a square contour such error was at the most 15 percent for the elastic crack tip field and less than 3 percent for an HRR field with a strain hardening exponent of N = 5. The additional error analysis provided in the following will show that the above far-field J-integral measurement procedure is indeed a reasonable approximation for the near-field J value, particularly in an HRR field.

Consider a rectangular contour, which is different from the square contour used in Ref. [8], around the crack tip as shown in the legend of Figure 2. The mode I plane stress linear elastic crack-tip displacements are:

$$u_x = \frac{K_I}{G}\sqrt{\frac{r}{2\pi}}\cos\frac{\theta}{2}\left[\frac{1-\nu}{1+\nu} + \sin^2\frac{\theta}{2}\right] \tag{5a}$$

$$u_y = \frac{K_I}{G}\sqrt{\frac{r}{2\pi}}\sin\frac{\theta}{2}\left[\frac{2}{1+\nu} - \cos^2\frac{\theta}{2}\right] \tag{5b}$$

$$W = \frac{1}{2}\sigma_{ij}\varepsilon_{iy}$$

where r and θ are the polar coordinates with the origin at the crack-tip and K_I is the mode I stress intensity factor. For a rectangular contour surrounding a Hutchinson-Rice-Rosengren (HRR) singular field as shown in the legend of Figure 3, the HRR stress, strain and displacement fields within this rectangular region can be expressed as [2, 3]

$$\sigma_{ij} = \sigma_i\left[\frac{J}{\alpha\sigma_o\varepsilon_o I_N r}\right]^{\frac{1}{N+1}} \tilde{\sigma}_{ij}(\theta) \tag{6a}$$

A-1

$$\varepsilon_{ij} = \alpha\varepsilon_o\left[\frac{J}{\alpha\sigma_o\varepsilon_o I_N r}\right]^{\frac{N}{N+1}} \tilde{\varepsilon}_{ij}(\theta) \qquad (6b)$$

$$u_i = \alpha\varepsilon_o r\left[\frac{J}{\alpha\sigma_o\varepsilon_o I_N r}\right]^{\frac{N}{N+1}} \tilde{u}_i(\theta) \qquad (6c)$$

where

I_N is a dimensionless constant which varies with plane stress or plane strain conditions

$\tilde{\sigma}_{ij}(\theta)$ $\tilde{\varepsilon}_{ij}(\theta)$ and $\tilde{y}_i(\theta)$ are dimensionless functions of θ and are obtained from Ref. [13].

For the approximate J_h and J_v, as represented by Equations (3) and (4), the needed σ_{yy} and W can be represented as:

$$\sigma_{yy} = \sigma_o \left(\frac{\varepsilon_{yy}}{\alpha\varepsilon_o}\right)^{1/N} \qquad (6e)$$

$$W = \frac{N}{N+1}\,\sigma_{yy}\,\varepsilon_{yy} \qquad (6f)$$

Equations (6e) and (6f) represents the plastic components of the power hardening stress-strain relation where the elastic components are assumed negligible. Equations (5) and (6) are used to evaluate the first and second terms of the integrand in Equation (1) or Equations (2) and (3) along a non-dimensionalized half rectangular contour, 0123456, as shown in Fig. 2. Results of these numerical integrations as one traverses along the half contour are plotted in Figures 2, 3, and 4. In these figures, the theoretically correct and the single-term J-integral values of Equations (2) and (3) are denoted as "theoretical" and "approximate" values, respectively. These figures show that the theoretical and the approximate summations of the incremental changes in J, ΔJ, or $\Sigma\Delta J$, along the contour before entering the last vertical segment of 56 are reasonably close. The nondimensionalized $J=\Sigma\Delta J$ values at point 4 shows about 15 percent difference between the theoretical and approximate $\Sigma\Delta J$ values in Fig. 2. Figure 2 shows that this error is generated during the last integration path or along the second vertical contour, line 56, indicating that the assumed uniaxial tension state is not a unreasonable approximation of the true state of elastic stresses along this line 56. The induced error in the elastic crack tip stress field can be reduced if line 56 is situated within the region of uniaxial tension or more specifically along a free boundary.

The results of Fig. 3 and 4 suggest that the approximate J as determined by the far-field solution, is reasonably correct when used in a HRR dominated crack tip region. The differences between $\Sigma\Delta J$ for the state of stress of the

HRR field along lines 56 or 456 are negligible and thus the approximate procedure of evaluating J works reasonably well.

EXPERIMENTAL APPROACH

White light moire interferometry [14] was used to obtain a single-frame record of the static and dynamic displacement fields surrounding the crack tip in slowly and rapidly fracturing 7075-T6, 2024-0 and 5052-H32 aluminum SEN specimens. Figures 5 and 6 show the optical system which utilizes a compensator grating of half frequency, f/2, where f = 1200 lines/mm, to illuminate the reference and specimen gratings of full and half frequencies, respectively. The achromatic light emerges from the compensator as monochromatic light beams at different diffraction angles and generates the same moire pattern for each wave length. The camera records the scalar sum of the light intensities associated with various wave lengths and thus much of the original white light intensity is recovered. When an incoherent light source is used, the gap between the reference and active gratings must be small. This white light moire interferometry provides the high sensitivity associated with high frequency gratings and the bright light source using a relatively simple experimental setup. The white light moire fringe patterns were recorded on a 35 mm camera without the Fourier optical filtering. A motor-driven camera provided up to 6 frames/second of fast sequential records of the moire fringes.

RESULTS

The fracture tests of the pin-loaded single-edge-notched specimens were conducted under incrementally increasing constant displacement loadings. The specimen configuration, material properties and the three material coefficients for the power hardening stress-strain relatins are shown in Table 1. These material properties indicate that aluminum 7075-T6 and 5052-H32 are essentially elastic-perfect plastic materials while 2024-0 is a strain hardening materials.

7075-T6 SEN Specimens

Figure 7 shows four typical white light moire interferometry fringe patterns in a fatigue precracked 7075-T6 aluminum SEN specimen which was subjected to increasing loads. Also shown in Figure 7 are two of the three contours used for estimating the J-values. The crack tip within the apparent caustics was located by the proven procedure of intersecting the maximum diameter of the caustics with the crack axis [9]. The log-log plot of the u_y displacement field in Figure 8 show that the small yield zone had little effect on the singular elastic crack tip stress which prevailed as far as 4 mm from the crack tip. This finding is in agreement with that reported previously [8].

The path independency of the approximate J-values along the three contours in two 7075-T6 SEN specimens were shown in Table 2 in Ref. [8,9] where the deviation in the J's was at the most 12 percent less along the inner and outer contours. As expected, the stress intensity factors computed from the approximate J agreed within 9 percent with computed stress itensity factors based on linear elastic fracture mechanics (LEFM) as shown in Table 1 of Ref. [8]. Figure 4 in Ref. [9] shows a 40 percent difference in the critical J_{c_s} of the two SEN specimens after small stable crack growths of 1.2 and 1.8 mm. This disconcerting difference could be due in part to the material anisotropy as evidenced by the 100 and 80 percent shear lips in the two specimens.

2024-0 SEN Specimens

Figure 9 shows four typical white light moire interferometry fringe patterns in a blunt notched 2024-0 aluminum SEN specimen with increasing load. The log-log plot of the u_y displacement field in Figure 10 show that the HRR field in this plastically yielded specimen existed in a small ring region inside of the 3 mm circle and outside of the caustic surrounding the crack tip. A similar finding involving a fatigue precracked 2024-0 aluminum SEN specimen indicate that the extent of the HRR field can be estimated by the same criterion used in estimating the extent of a linearly elastic crack tip field.

The path independency of the approximate J's evaluated along the three contours is shown by Table 2 as well as Table 3 in Ref. [8] where the maximum difference in J's is about 4 percent. Figure 11 shows the approximate J resistance curves for fatigue precracked and blunt notched specimens. Figure 12 shows the crack tip opening displacement (CTOD) resistance curves for the same two specimens. Both the approximate J and the CTOD resistance curves are relatively insensitive to the notch bluntness possibly due to the large plastic yielding which dominates the crack tip region prior to stable crack growth. Note that the crack instability was not attained during these stable crack growths.

5052-H32 SEN Specimens

Figure 13 shows four typical white light moire interferometry patterns in a fatigue precracked 5052-H32 aluminum SEN specimen with increasing load. Figures 14 and 15 show the log-log plots of the u_y displacement fields in a fatigue precracked and blunt notched specimens, respectively where a slope of 1/16 was expected if the HRR field was to prevail in the vicinity of the crack tip. The unexpected slope of 1/2 indicates that the HRR field does not exists in this grossly yielded SEN specimens, particularly ahead of the crack tip or θ less than 60. Where plastic yielding is less dominant, i.e. for θ larger than 90°, the slopes of these displacment curves approach 1/16 as expected from the normal strain contours which are shown in Figure 16.

The path independency of the approximate J's are shown in Table 3 in Ref. [9] where the maximum difference between the J's of different contours is 5 percent. Figure 17 shows the approximate J resistance curves for fatigue precracked and blunt notched specimens. Figure 18 shows the CTOD resistance curves for the same two specimens. Again the gross plastic yielding prior to stable crack growth had apparently overwhelmed any notch bluntness effect which may have existed prior to plastic yielding.

DISCUSSIONS

The J-resistance curves for small stable crack growths in two 7075-T6 specimens [9] can be compared with the J estimated for a small scale yielding condition using a Dugdale model [15]. While the theoretical analysis was restricted to a specimen geometry of $a_i/w = 0.25$, the noticeable differences between the theoretical and experimental results can be attributed more to the initial stable crack growth without increase in applied J and is associated with the minute crack tip blunting in this somewhat brittle material.

Otherwise the agreement between the theoretical and experimental results are excellent.

As a further validation of the J-estimation procedure described above, the approximate J was evaluated along a rectangular contour, which did not enclose the crack tip, in a fatigue precracked 5052-H32 aluminum SEN specimen [9]. The resultant J, which theoretically should have vanished, was 0.2 percent of the corresponding approximate J.

The path independency of the approximate J's in the presence of small stable crack growth is in agreement with known numerical studies involving A533B steel [7]. An experimental study of this path independency under larger crack extension of 20 to 30 mm is being conducted.

The vanishing HRR field under large plastic yielding of a material with a relative large strain hardening exponent, i.e. N=15, was surprising.

CONCLUSIONS

The accuracy of the approximate J's evaluated along oblong rectangular contours in the elastic and the HRR crack tip fields was assessed. Induced errors in the approximate J can be reduced to less than 1 percent if the last vertical contour is taken along the free boundary of a SEN specimen.

The path independency of the approximate J's in the presence LEFM and elastic-plastic stress fields was demonstrated experimentally in 7075-T6, 2024-0 and 5052-H32 SEN specimens with small stable crack growth of 1 to 2 mm.

HRR field does not exist in a ductile material with relatively large strain hardening exponent, i.e. N=15.

The approximate J and the CTOD resistance curves for 2024-0 and 5052-H32 specimens for small crack extension were established. These curves showed little sensitivity to the notch tip acuity due large plastic yielding.

ACKNOWLEDGEMENT

The work reported here was completed under ONR Contract N00014-85-K-0187. The authors wish to acknowledge the support and encouragement of Dr. Yapa Rajapakse, ONR, during the course of this investigation.

REFERENCES

1. Rice, J.R., "A Path Independent Integral and the Approximate Analysis of Strain Concentration by Notches and Cracks," Journal of Applied Mechanics, Vol. 35, Series E, June 1968, pp. 379-386.

2. Hutchinson, J.W., "Plastic Stress and Strain Fields at a Crack Tip," Journal of Mechanics and Physics of Solids, Vol. 16, 1968, pp. 337-347.

3. Rice, J.R. and Rosengren, G.F., "Plane Strain Deformation Near a Crack Tip in a Power-Law Hardening Material," Journal of Mechanics and Physics of Solids, Vol. 16, 1968, pp. 1-12.

4. Landes, J.D. and Begley, J.A., "The Effect of Specimen Geometry on J," Fracture Toughness, ASTM ATP 514, 1972, pp. 24-39.

5. Rice, J.R., Paris, P.C. and Merkle, J.G., "Some Further results of J-Integral Analysis and Estimates," Progress in Flaw Growth and Fracture Toughness Testing, ASTM STP 536, 1973, pp. 231-245.

6. Kumar, V., German, M.D. and Shih, C.F., "An Engineering Approach to Elastic-Plastic Fracture Analysis," NP-1931, Research Project 1237-1, Electric Power Research Insitute, July 1981.

7. Shih, S.F., deLorenzi, H.G. and Andrews, W.R., "Studies on Crack Initiation and Stable Crack Growth," Elastic-Plastic Fracture, ed. by J.D. Landes, J.A. Begley and G.A. Clarke, ASTM STP 668, 1979, pp. 65-120.

8. Kang, B.S.-J., Kobayashi, A.S. and Post, D., "Stable Crack Growth in Aluminum Tensile Specimens," to be published in Experimental Mechanics.

9. Kang, B.S.-.J and Kobayashi, A.S., "J-resistance Curves of Aluminum SEN Specimens," to be published in Experimental Mechanics.

10. King, R.B., and Herrmann, G., "Nondestructive Evaluatin of the J amd M Integrals," Journal of Applied Mechanics, Vol. 48, pp. 83-87, 1981.

11. Read, D.T., and McHenry, H.I., "Strain Dependence of the J-Contour Integral in Tensile Panels," Advance in Fracture Research, edited by D. Francois et al., pp. xx-xx, 1980.

12. Read, D.T., "Experimental Method for Direct Evaluation of the J Contour Integral," Fracture Mechanics, ASTM STP 791, pp. 199-213, 1983.

13. Shih, C.F., "Tables of Hutchinson-Rice-Rosengren Singular Field Quantities," MRL E-147, Materials Research Laboratory, Borwn University, 1983.

14. Post, D., "Moire Interferometry with White Light," Applied Optics, Vol. 18, No. 24, pp. 4163-4167, 1979.

15. Budiansky, B., and Sumner, E.E., Jr., "On Size Effects in Plane Stress Crack-Growth Resistance," to be published in the Developments in Mechanics, Vol. 19, Proc. of the 19th Midwestern Mech. Conf., Ohio State, Sept. 9-11, 1987.

Table 1 Test Material Properties

Aluminum	Yield Stress (MPa)	Young's Modulus (MPa)	α	N
7075-T6	504	71,800	0.1	47
2024-0	64	72,300	0.35	5
5052-H32	190	70,200	0.4	15

$$\varepsilon_{yy} = \frac{\sigma_{yy}}{E_o} + \alpha\frac{\sigma_{yy}}{E}\left(\frac{\sigma_{yy}}{\sigma_o}\right)^{N-1}$$

Table 2 Approximate J Values for Three Different Contours in Blunt Notched 2024-O Aluminum SEN Specimen. Specimen No. KJD1.

Frame No.	Applied Load (MN)	Crack Length (mm)	Approximate J Contour #1* (MPa m)	#2 (MPa m)	#3 (MPa m)
1	1.01	1.40	0.70×10^{-3}	0.70×10^{-3}	0.69×10^{-3}
2	1.57	1.48	4.38×10^{-3}	4.3×10^{-3}	$4.38\times^{-3}$
3	1.72	1.58	7.37×10^{-3}	7.33×10^{-3}	7.34×10^{-3}
4	1.80	1.62	8.59×10^{-3}	8.5×10^{-3}	8.53×10^{-3}
5	2.10	1.76		13.3×10^{-3}	12.6×10^{-3}
6	2.30	1.96		15.7×10^{-3}	14.1×10^{-3}

* Near-field contour
** Far-field contour

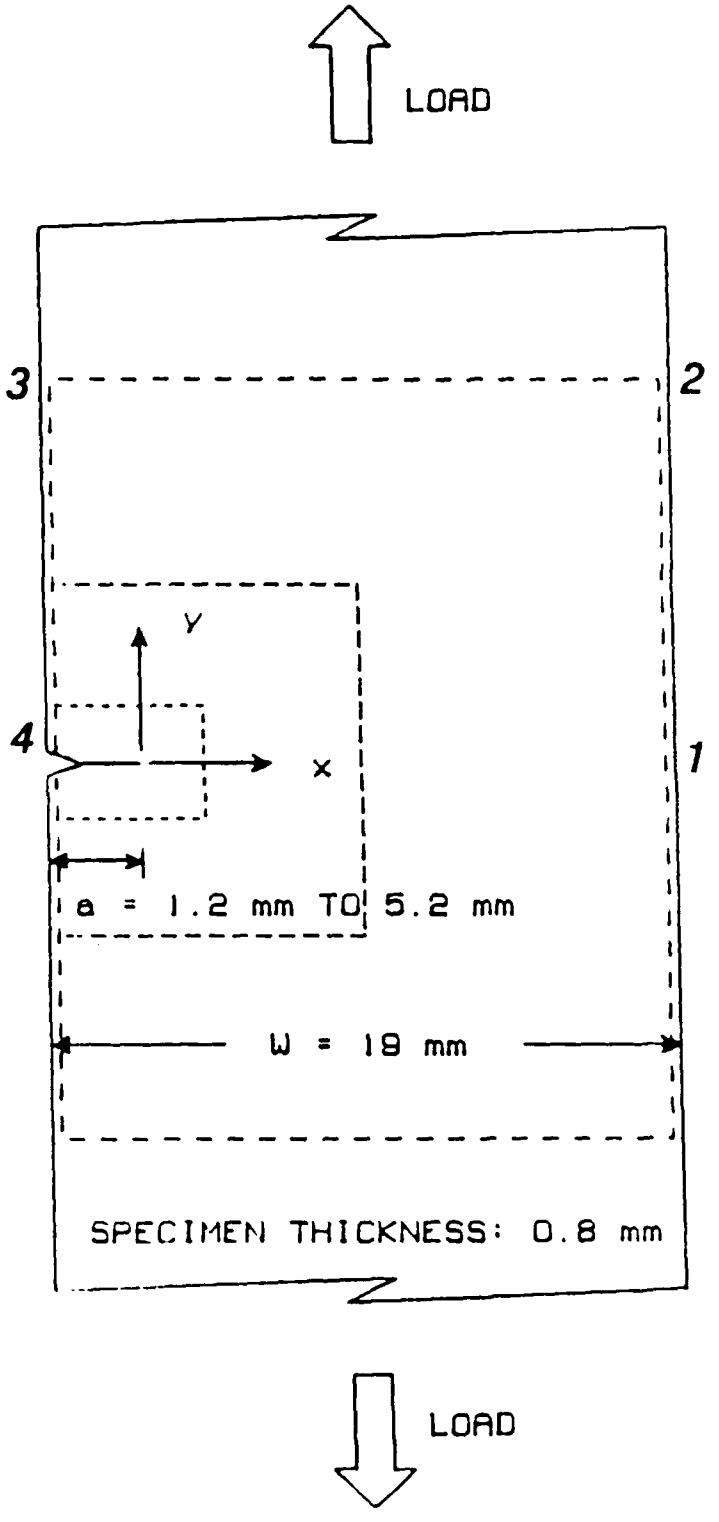

Figure 1 Single Edge Notched (SEN) Specimen and Contours for J Evaluation.

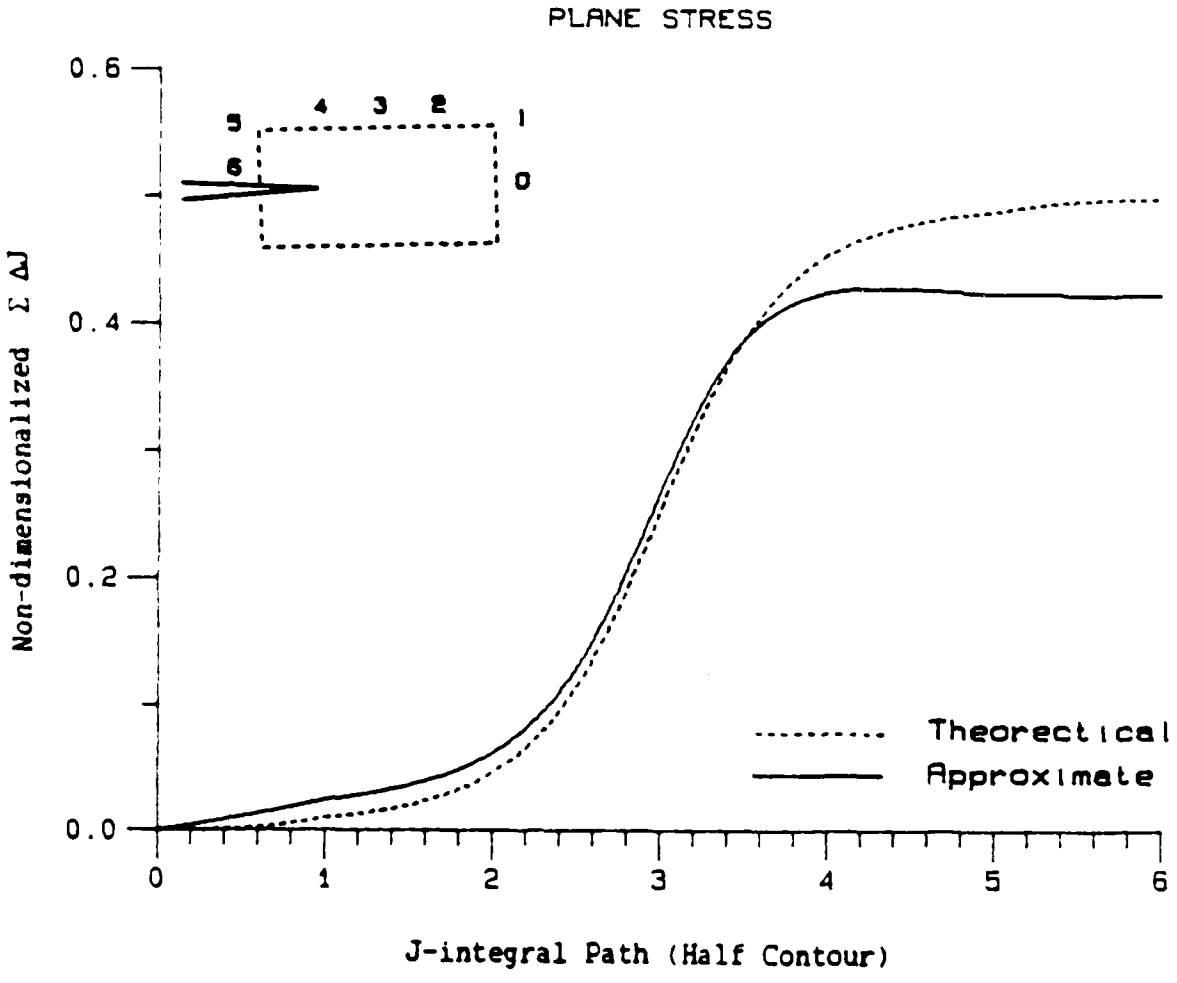

Figure 2 Theoretical and Approximate J Values, $\Sigma\Delta J$. Plane Stress Linear Elastic Crack Tip Field. $\nu = 0.3$.

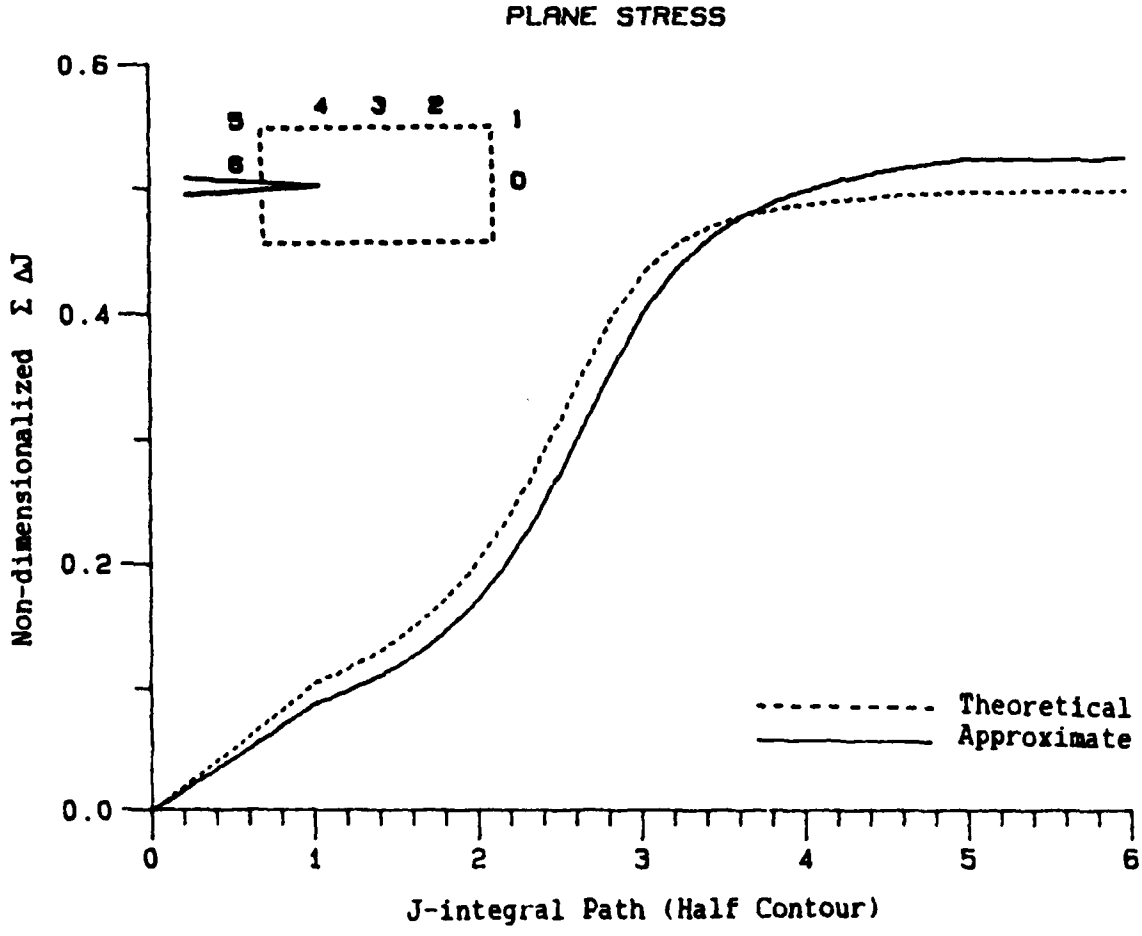

Figure 3 Theoretical and Approximate J Values, $\Sigma\Delta J$. Plane Stress, HRR Field with N = 5.

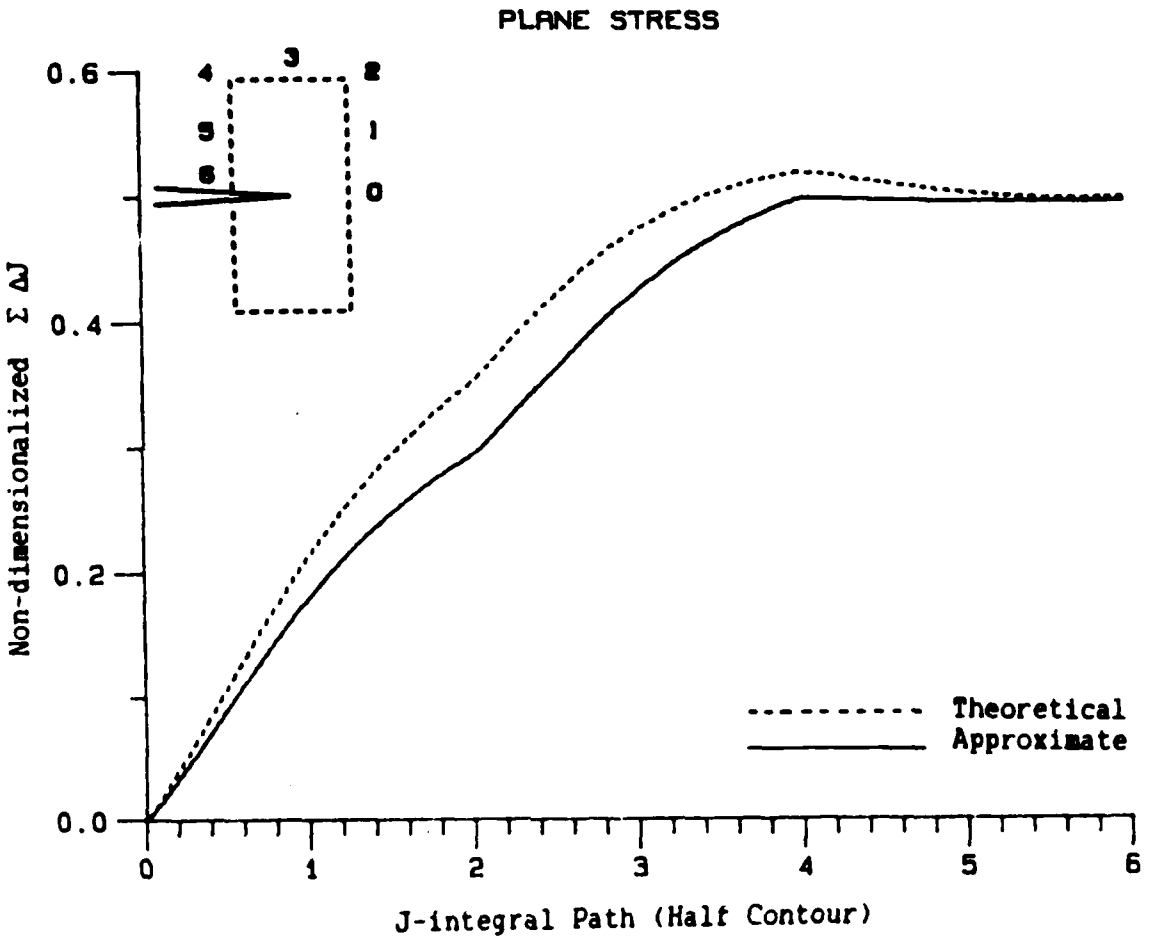

Figure 4 Theoretical and Approximate J Values, $\Sigma\Delta J$. Plane Stress, HRR Field with N = 5

$$\sin \alpha = \frac{1}{2} \lambda f$$

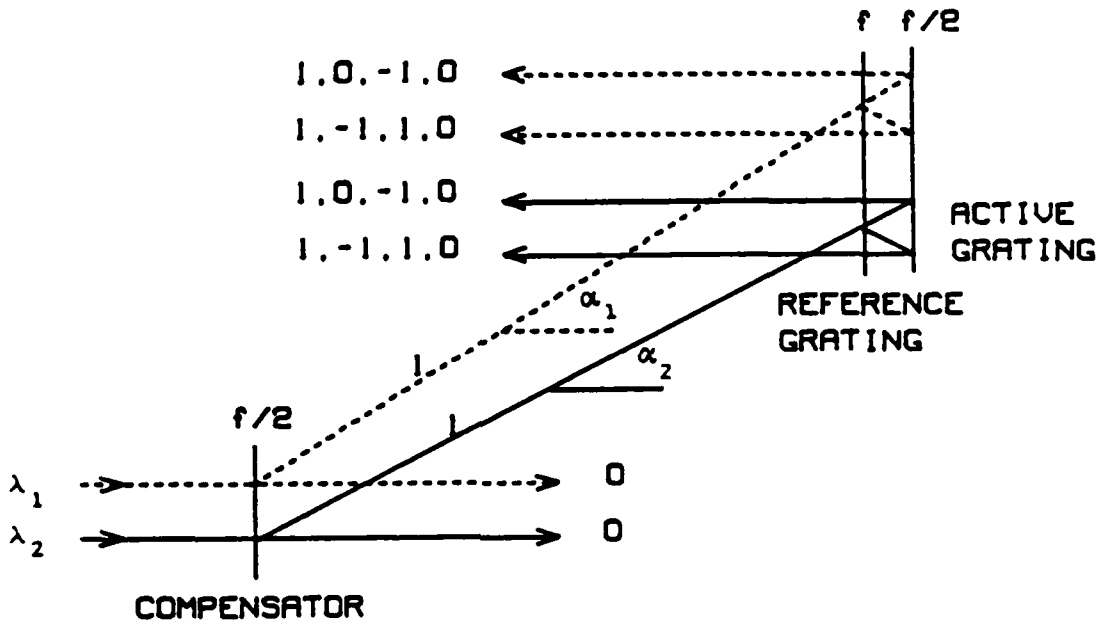

Figure 5 Optical Paths for White Light Moire Interferometry (f = 1200 lines/mm).

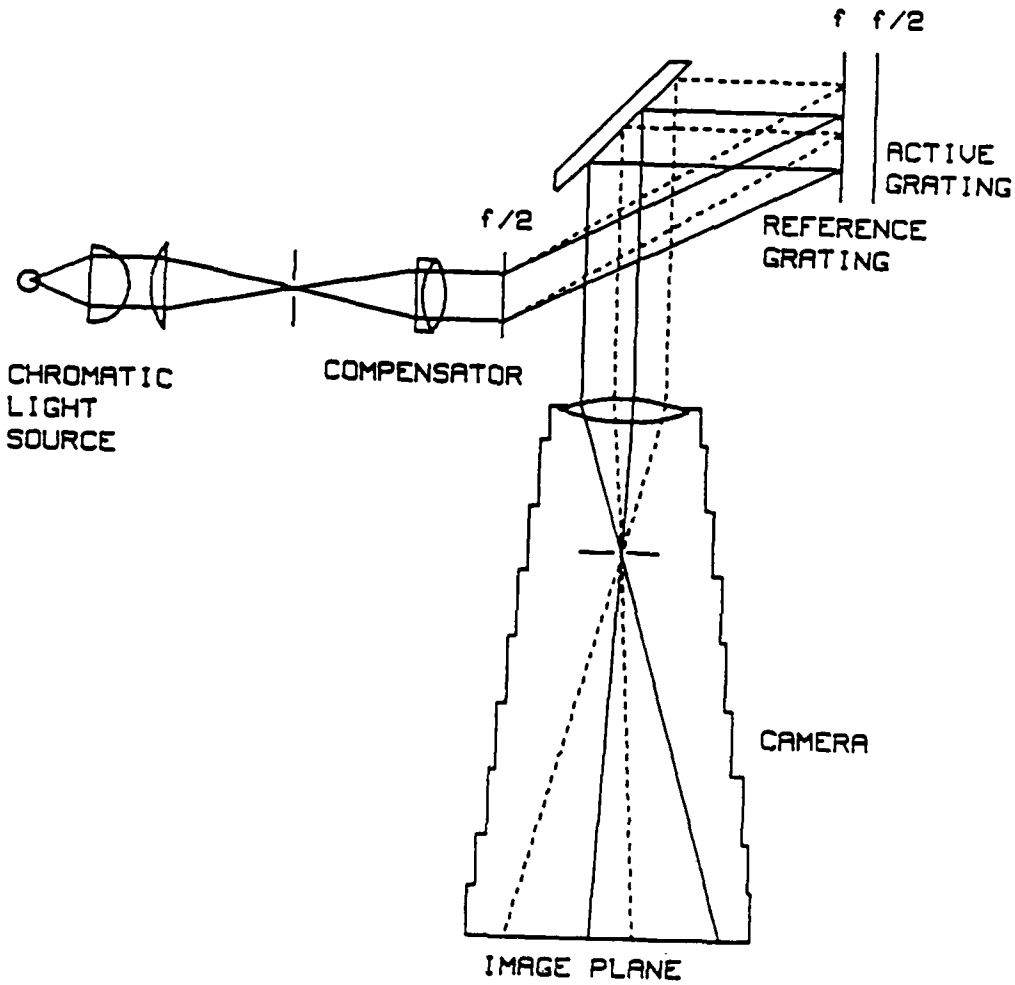

Figure 6 Moire Fringe Patterns of a Fatigue Precracked 7075-T6 Aluminum SEN Specimen under Increasing Load. Specimen No. KJA2. Initial a = ? mm.

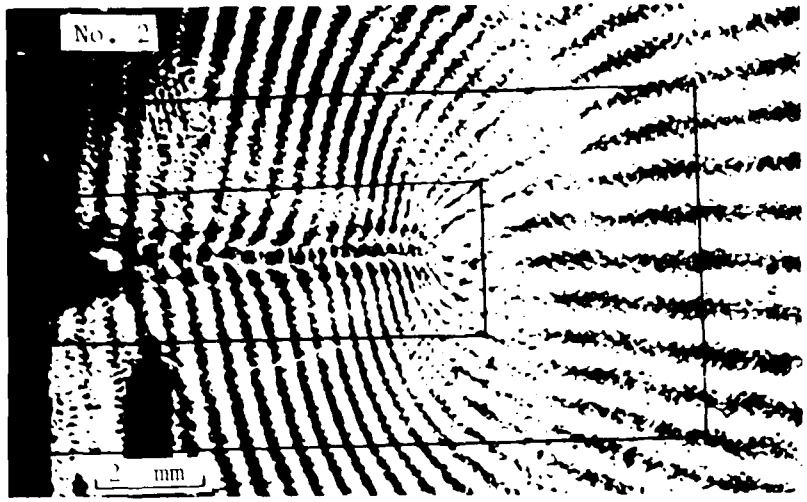

Applied Load: 1.38 KN
Crack Extension: 0 mm

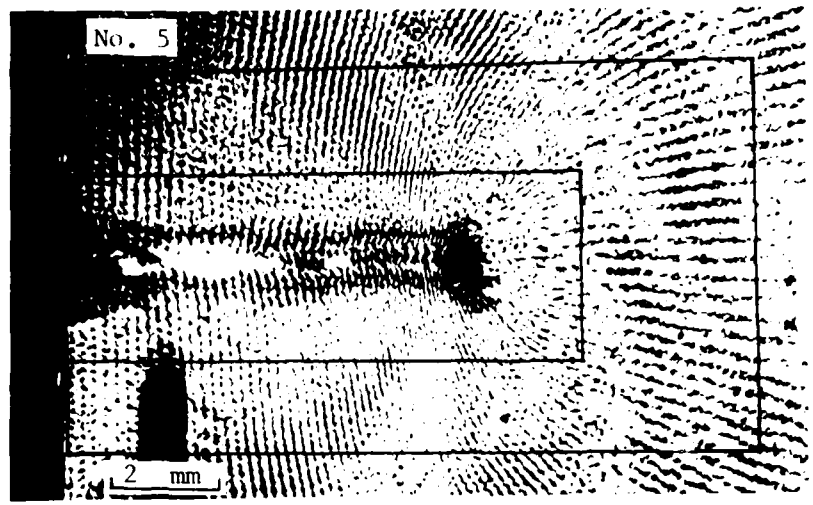

Applied Load: 2.12 KN
Crack Extension: 0.35 mm

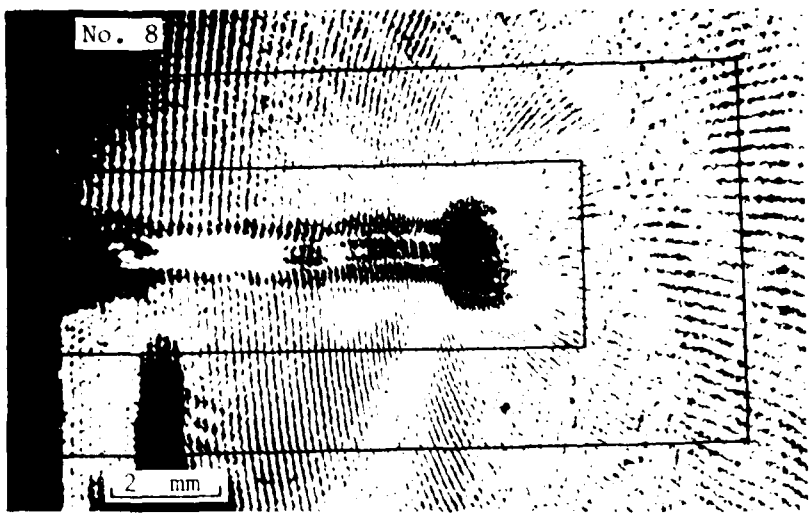

Applied Load: 2.70 KN
Crack Extension: 0.62 mm

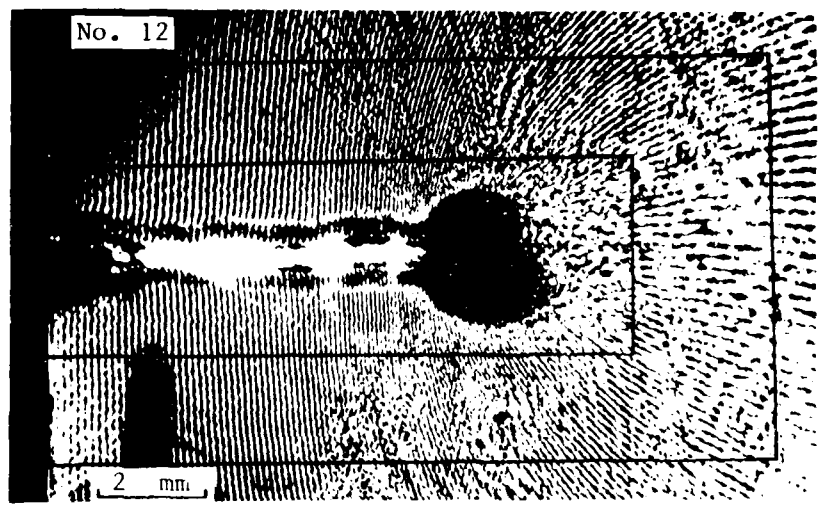

Applied Load: 3.22 KN
Crack Extension: 1.16 mm

Figure 7 u_y-Displacement Field. Fatigue Precracked 7075-T6 Aluminum SEN Specimen. Frame No. KJA2-2.

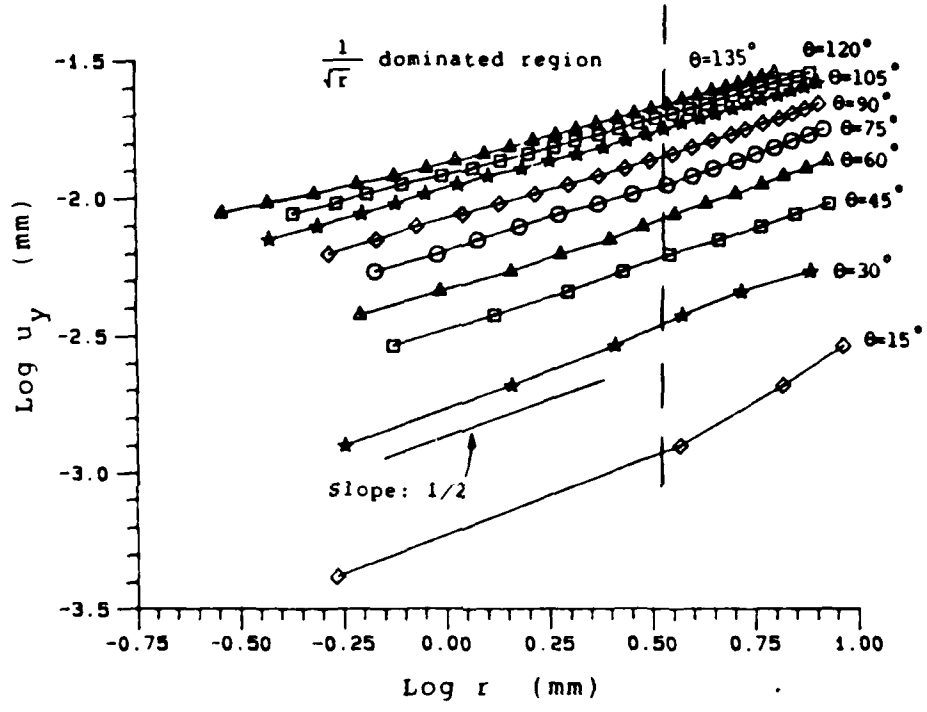

Figure 8 u_y-Displacement Field. Fatigue Precracked 7075-T6 Aluminum SEN Specimen. Frame No. KJA2-2.

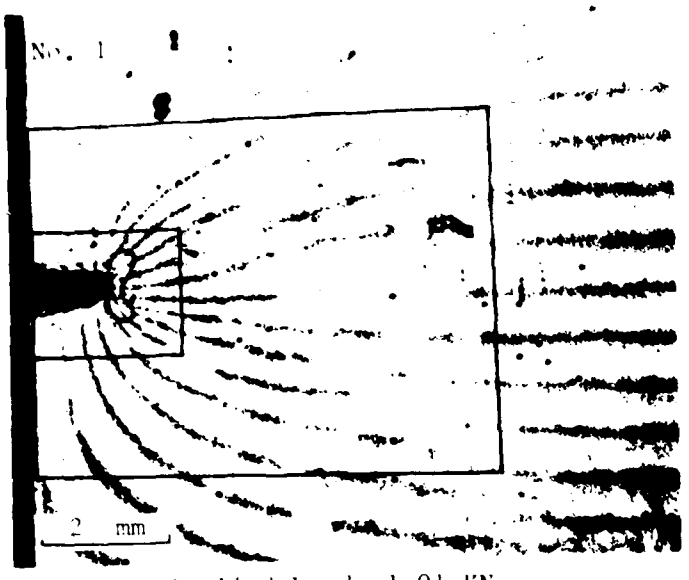

Applied Load: 1.01 KN
Crack Extension: 0 mm

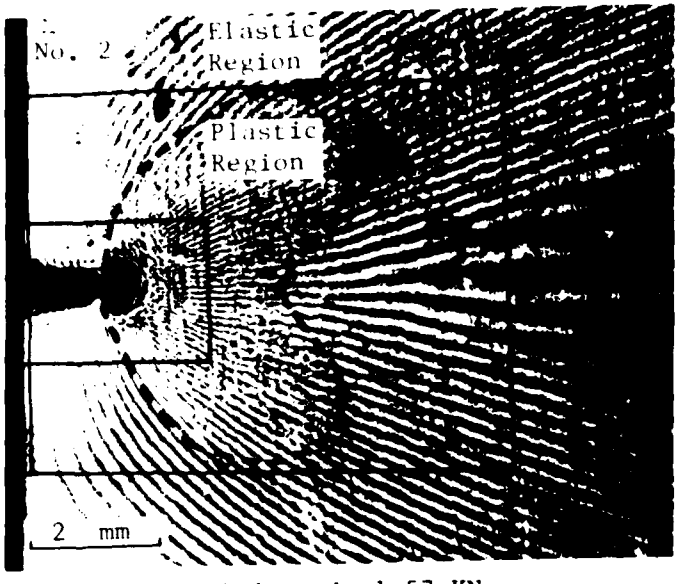

Applied Load: 1.57 KN
Crack Extension: 0.08 mm

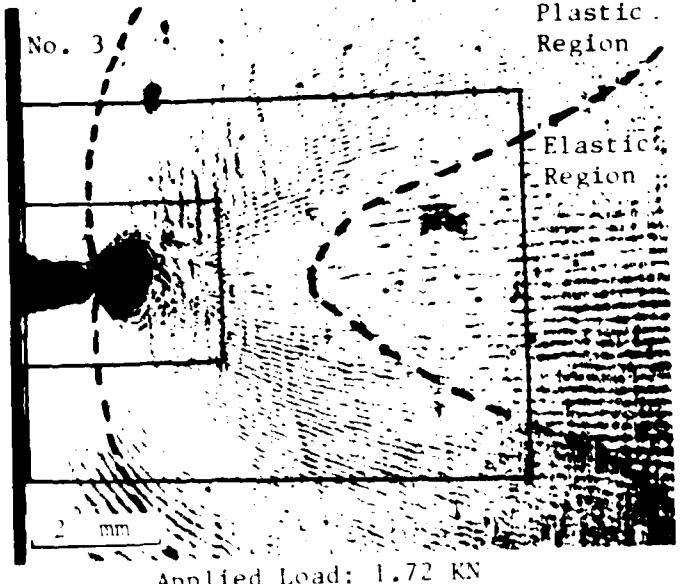

Applied Load: 1.72 KN
Crack Extension: 0.18 mm

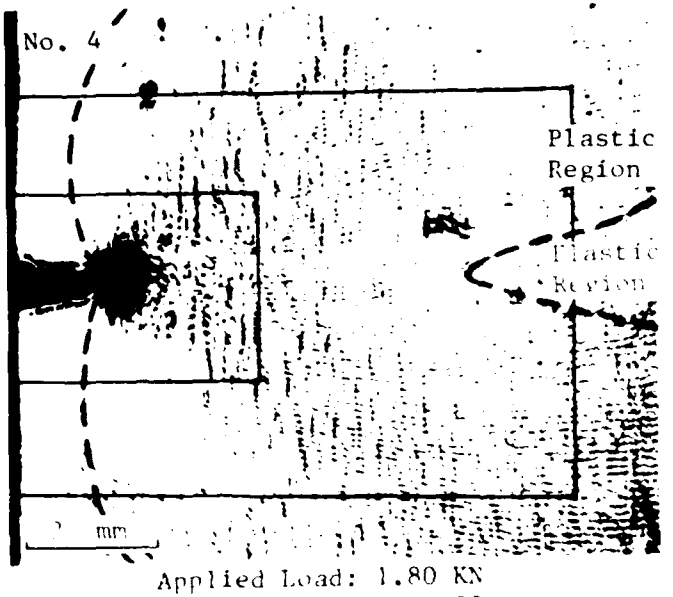

Applied Load: 1.80 KN
Crack Extension: 0.22 mm

Figure 9 Moire Patterns in Blunt-Notched 2024-0 SEN Specimen under Increasing Load.

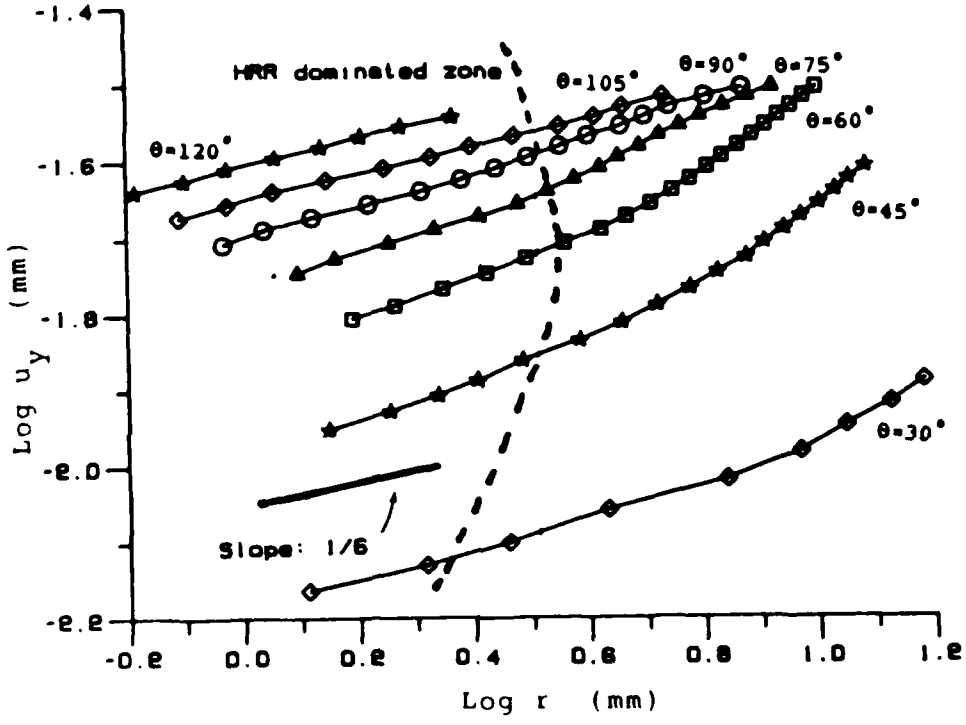

Figure 10 u_y Displacement Field. Blunt Notched 2024-0 Aluminum SEN Specimen. Frame No. KJD1-2.

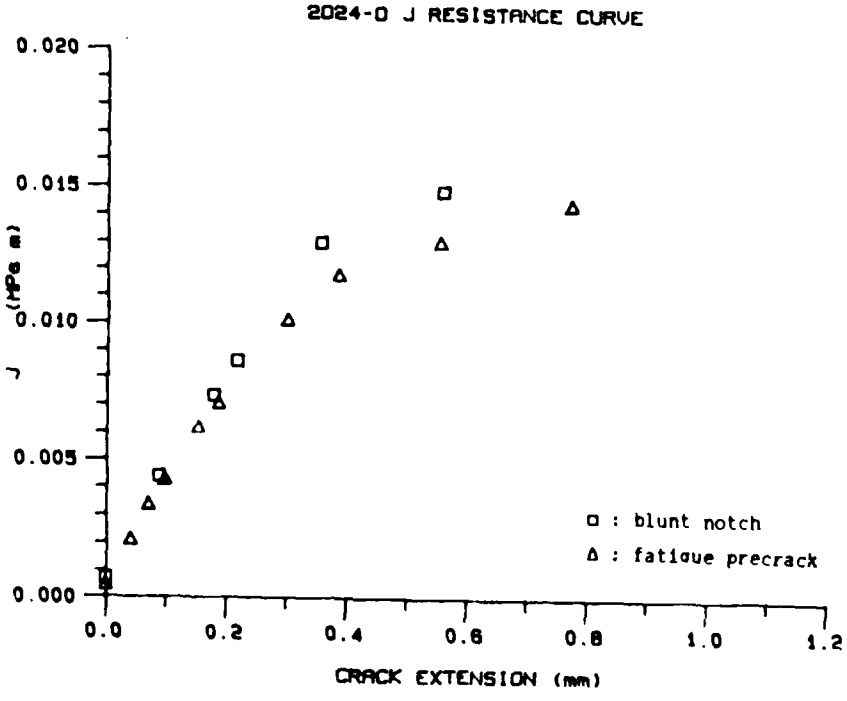

Figure 11 Approximate Resistance Curves 2024-0 Aluminum SEN Specimens. Specimen No. KJC1: Fatigue Precrack with Initial Crack Length 1.6 mm. Specimen No. KJD1: Blunt Notch with Initial Crack Length 1.2 mm.

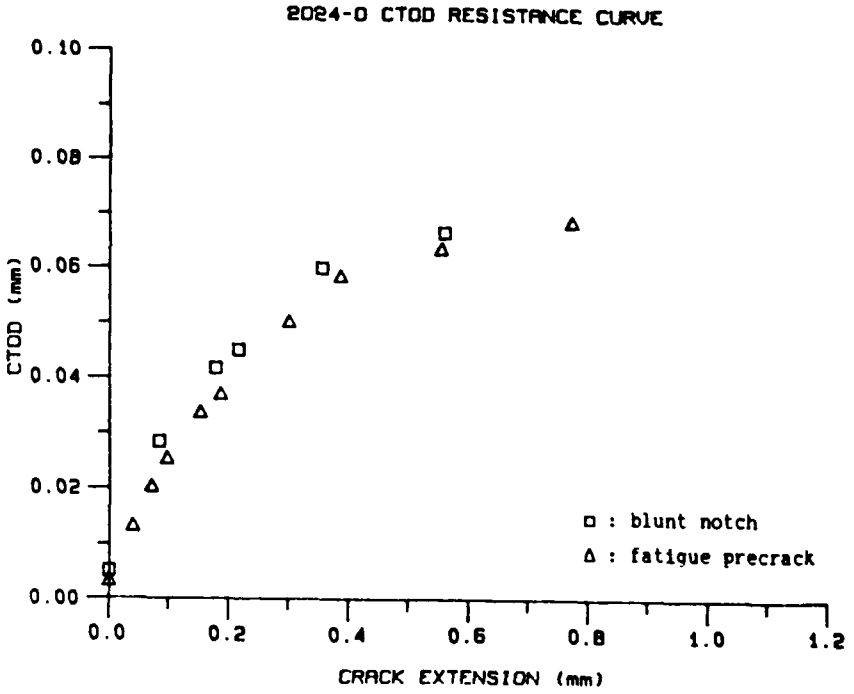

Figure 12 CTOD Resistance Cruves, 2024-0 Aluminum SEN Specimens. Specimen No. KJC1: Fatigue precracked with Initital Crack Length 1.6 mm. Specimen No. KJD1: Blunt Notched with Initial Crack Length 1.2 mm.

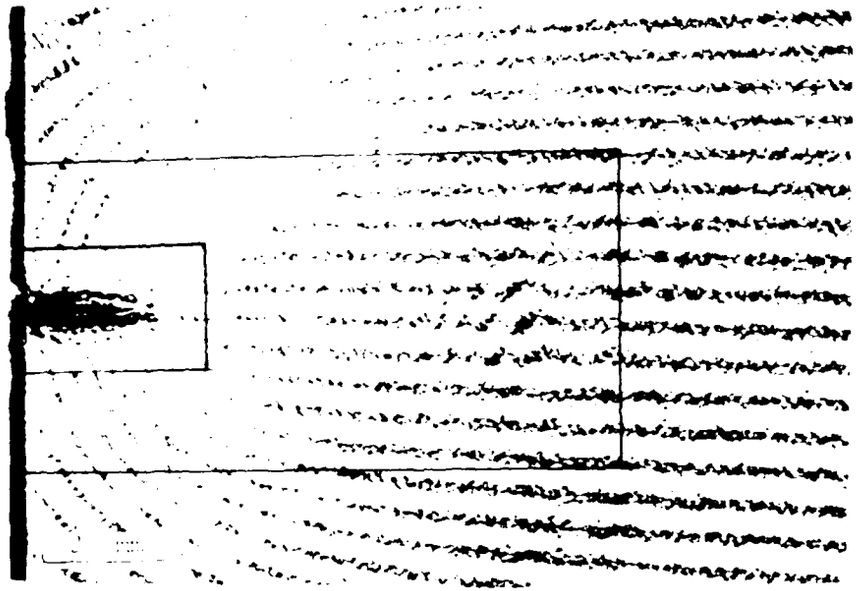

Applied Load: 1.23 KN
Crack Extension: 0 mm

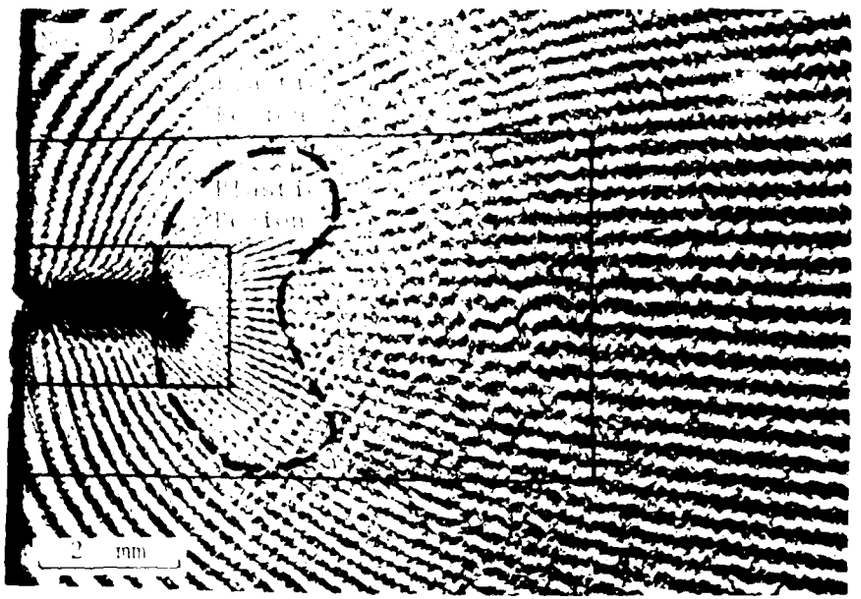

Applied Load: 1.78 KN
Crack Extension: 0.18mm

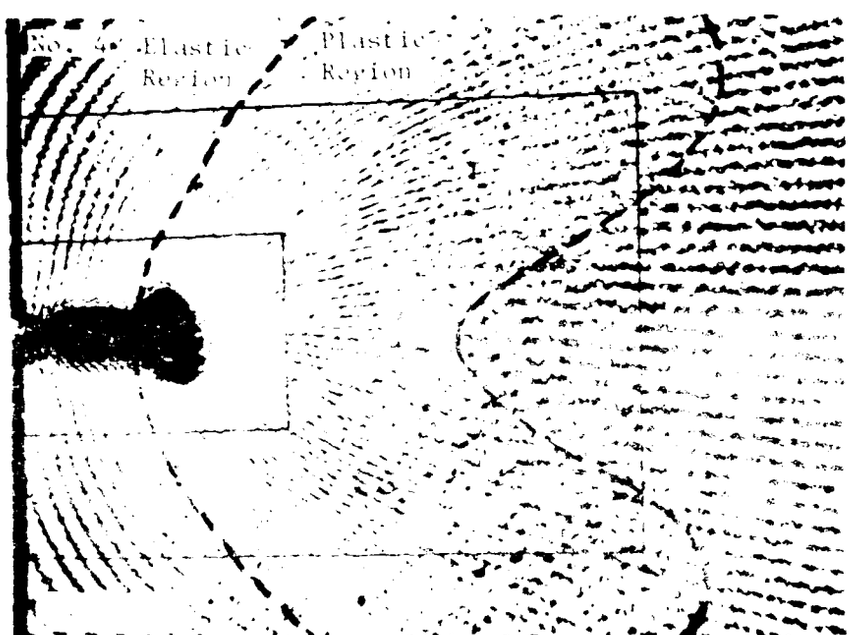

Applied Load: 1.89 KN
Crack Extension: 0.26 mm

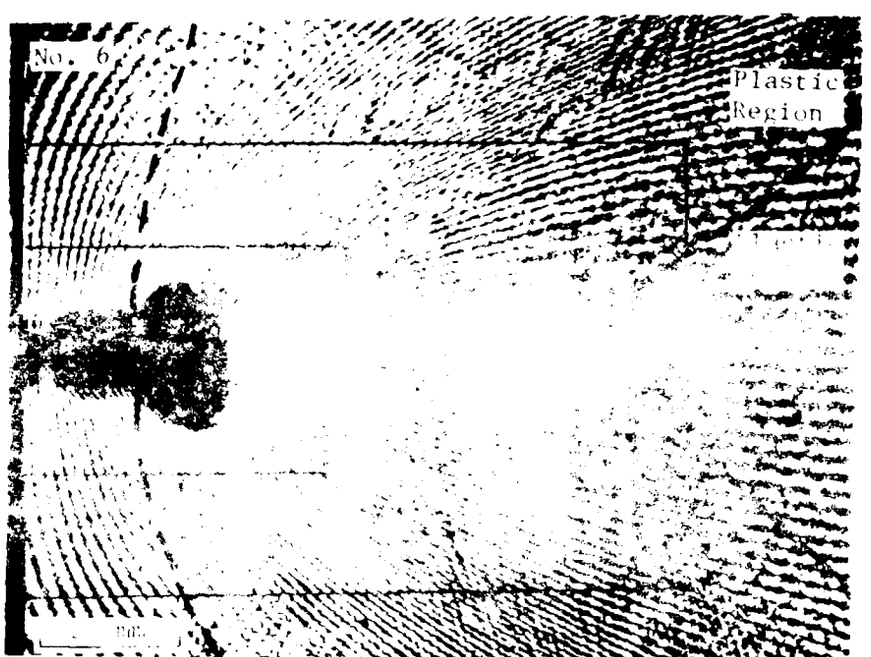

Applied Load: 2.02 KN
Crack Extension: 0.51 mm

Figure 13 Moire Fringe Patterns of a Fatigue Precracked 5052-H32 Aluminum SEN

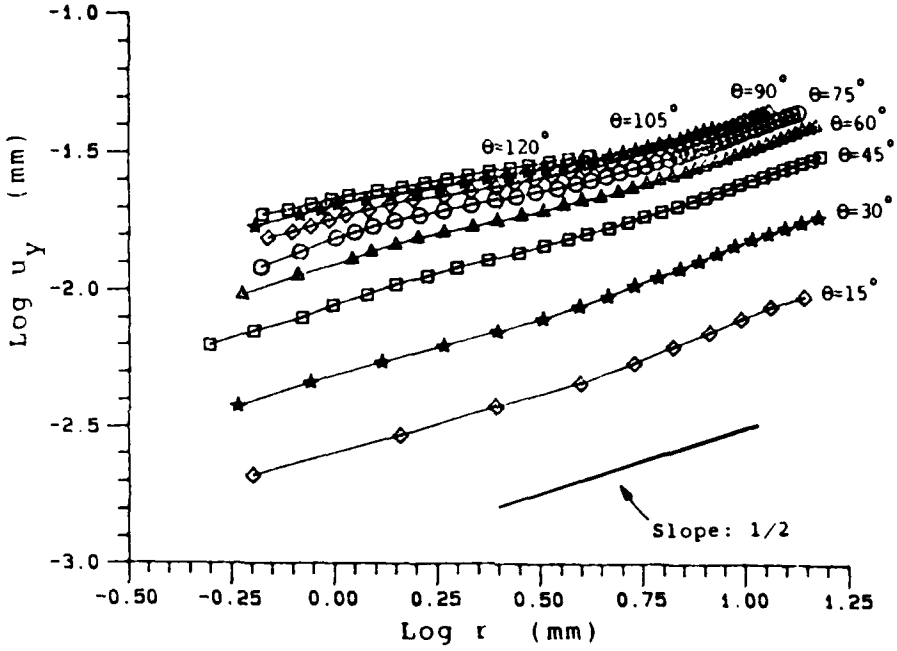

Figure 14 u_y-Displacement Field. Fatigue Precracked 5052-H32 Aluminum SEN Specimen. Frane No. KJG1-4.

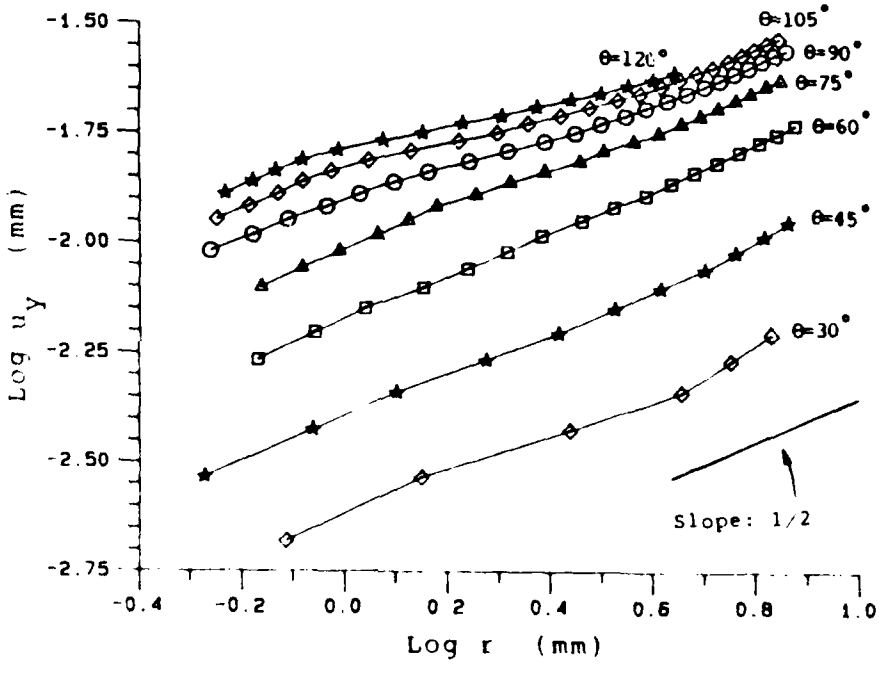

Figure 15 u_y-Displacement field. Blunt Notch 5052-H32 Aluminum SEN Specimen. Frame No. KJH1-3.

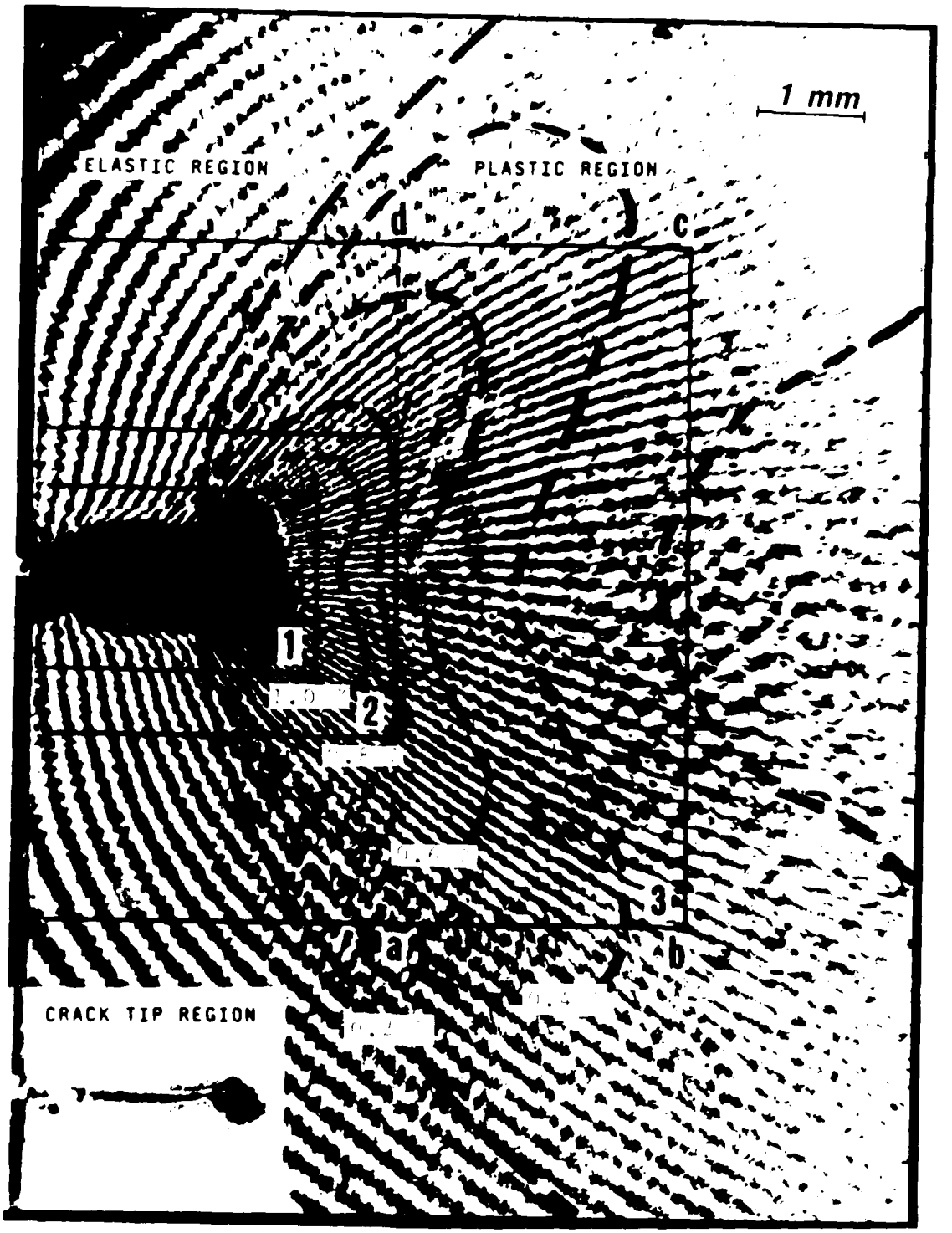

Figure [illegible] Normal Strain Contours in Fatigue Precracked 5052-H32 Aluminum Specimens. Specimen No. FUG1-X.

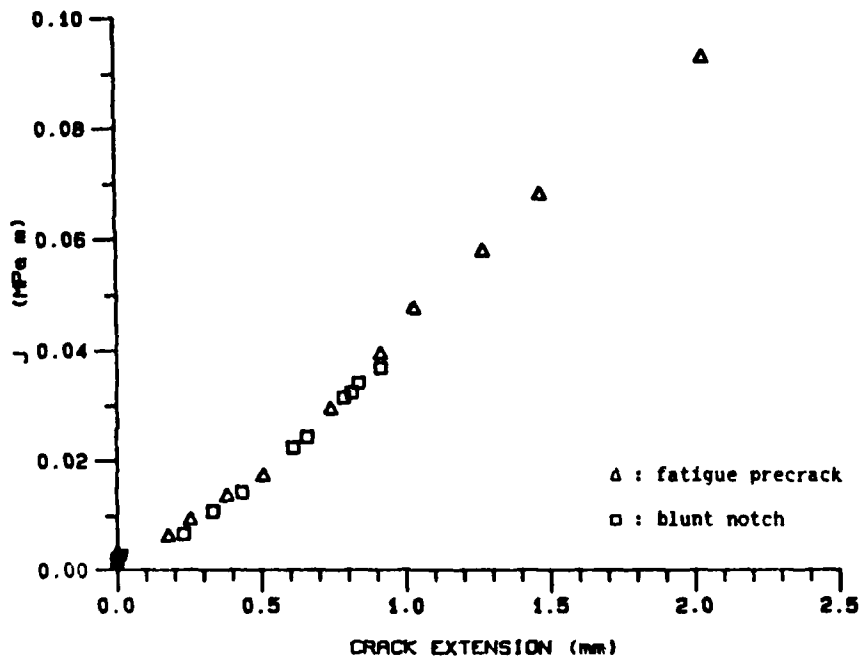

Figure 17 Approximate Resistance Curves, 5052-H32 Aluminum SEN Specimens. Specimen No. KJG1, Fatigue Precracked with Initial Crack Length 1.6 mm. Specimen No. KJH1, Blunt Notched with Initial Crack Length 0.8 mm

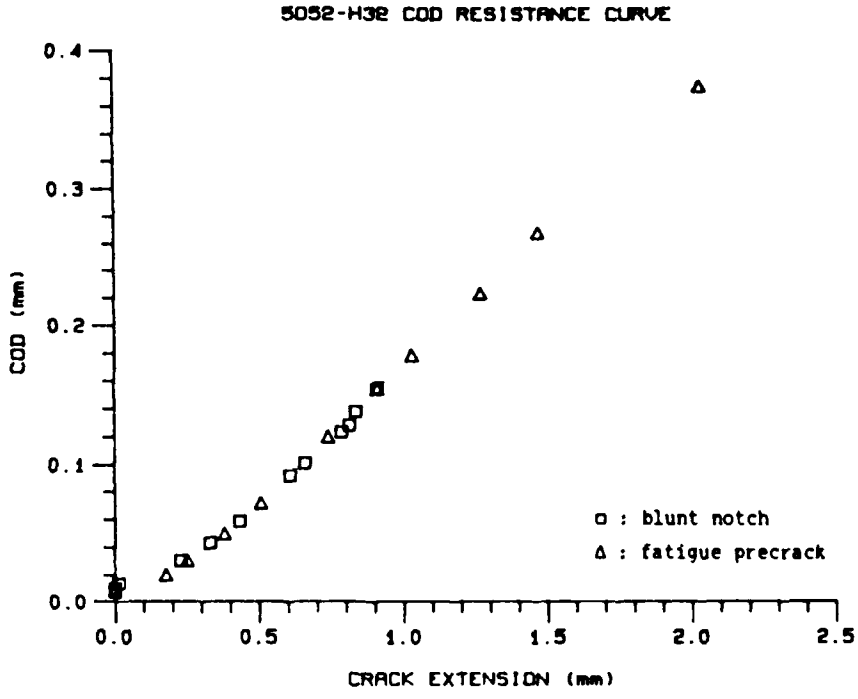

Figure 18 CTOD Values versus Crack Extension, 5052-H32 Aluminum SEN Specimens. Specimen No. KJG1, Fatigue Precracked with Initial Crack Length 1.6 mm. Specimen No. KJH1, Blunt Notched with Initial Crack Length 0.8 mm.

JMB MASTER MAILING LIST
UPDATED 7/86

Office of Naval Research
800 N. Quincy Street
Arlington, VA 22217-5000
Attn: Code 1132SM (4 copies)

Office of Naval Research
800 N. Quincy Street
Arlington, VA 22217-5000
Attn: Code 1131

Defense Documentation Center (4 copies)
Cameron Station
Alexandria, VA 22314

Naval Research Laboratory
Washington, DC 20375
Attn: Code 6000

Naval Research Laboratory
Washington, DC 20375
Attn: Code 6300

Naval Research Laboratory
Washington, DC 20375
Attn: Code 6380

Naval Research Laboratory
Washington, DC 20375
Attn: Code 5830

Naval Research Laboratory
Washington, DC 20375
Attn: Code 6390

Naval Research Laboratory
Washington, DC 20375
Attn: Code 2620

David W. Taylor Naval Ship
Research & Development Center
Annapolis, MD 21402
Attn: Code 28

David W. Taylor Naval Ship
Research & Development Center
Annapolis, MD 21402
Attn: Code 2812

David W. Taylor Naval Ship
Research & Development Center
Annapolis, MD 21402
Attn: Code 2814

David W. Taylor Naval Ship
Research & Development Center
Bethesda, MD 20084
Attn: Code 1700

David W. Taylor Naval Ship
Research & Development Center
Bethesda, MD 20084
Attn: Code 1720

David W. Taylor Naval Ship
Research & Development Center
Bethesda, MD 20084
Attn: Code 1720.4

Naval Air Development Center
Warminster, PA 18974
Attn: Code 6043

Naval Air Development Center
Warminster, PA 18974
Attn: Code 6063

Naval Surface Weapons Center
White Oak, MD 20910
Attn: Code R30
Technical Library

Naval Surface Weapons Center
Dahlgren, VA 22448
Attn: Technical Library

Naval Civil Eng Library
Port Hueneme, CA 93043
Attn: Technical Library

Naval Underwater Systems Center
New London, CT 06320
Attn: Code 44
Technical Library

Naval Underwater Systems Center
Newport, RI 02841
Attn: Technical Library

Naval Weapons Center
China Lake, CA 93555
Attn: Technical Library

NRL/Underwater Sound Reference Det.
Orlando, FL 32856
Attn: Technical Library

Chief of Naval Operations
Department of the Navy
Washington, DC 20350
Attn: Code OP-098

Commander
Naval Sea Systems Command
Washington, DC 20362
Attn: Code 05B25

Commander
Naval Sea Systems Command
Washington, DC 20362
Attn: Code 05B26

Commander
Naval Sea Systems Command
Washington, DC 20362
Attn: Code 09B31

Commander
Naval Sea Systems Command
Washington, DC 20362
Attn: Code 55Y

Commander
Naval Sea Systems Command
Washington, DC 20362
Attn: Code 55Y2

Commander
Naval Air Systems Command
Washington, DC 20361
Attn: Code 03D

Commander
Naval Air Systems Command
Washington, DC 20361
Attn: Code 7226

Commander
Naval Air Systems Command
Washington, DC 20361
Attn: Code 310A

Commander
Naval Air Systems Command
Washington, DC 20361
Attn: Code 3108

US Naval Academy
Mechanical Engineering Dept.
Annapolis, MD 21402

Naval Postgraduate School
Monterey, CA 93940
Attn: Technical Library

Mr. Jerome Persh
Stf Specit for Matls & Struct
OUSDR&E, The Pentagon
Room 3B1089
Washington, DC 20301

Professor J. Hutchinson
Harvard University
Div of Applied Sciences
Cambridge, MA 02138

Professor B.M. Gallagher
Worcester Polytechnical Institute
Worcester, MA 01609

Dr. Harold Liebowitz, Dean
School of Engr & Applied Sci
George Washington University
Washington, DC 20052

Professor G.T. Mase
Vanderbilt University
Dept of Mech & Matls Engr
Nashville, TN 37235

Professor Albert S. Kobayashi
Dept of Mechanical Engineering
University of Washington
Seattle, WA 98195

Professor L.B. Freund
Brown University
Division of Engineering
Providence, RI 02912

Professor B. Budiansky
Harvard University
Division of Applied Sciences
Cambridge, MA 02138

Professor S.N. Atluri
Georgia Institute of Technology
School of Engr & Mechanics
Atlanta, GA 30332

Professor J. Duffy
Brown University
Div of Engineering
Providence, RI 02912

Professor J.D. Achenbach
Northwestern University
Dept of Civil Engineering
Evanston, IL 60201

Professor F.A. McClintock
Dept of Mechanical Engineering
Massachusetts Institute of Technology
Cambridge, MA 02139

Professor D.M. Parks
Dept of Mechanical Engineering
Massachusetts Institute of Technology
Cambridge, MA 02139

Dr. M.F. Kanninen
Southwest Research Institute
PO Drawer 28510
6220 Culebra Road
San Antonio, TX 78284

Professor F.P. Chiang
Dept of Mechanical Engr
State U of NY at Stony Brook
Stony Brook, New York 11794

Professor S.S. Wang
Dept of Theoretical & Applied Mechs
University of Illinois
Urbana, Illinois 61801

Professor Y. Weitsman
Civil Engr Department
Texas A&M University
College Station, Texas 77843

Professor I.M. Daniel
Dept of Mechanical Engr
Illinois Institute of Technology
Chicago, Illinois 60616

Professor C.T. Sun
School of Aeronautics & Astronautics
Purdue University
W. Lafayette, IN 47907

Professor J. Achenbach
Dept of Mech Engr & Mechanics
Drexel University
Philadelphia, PA 19104

Professor T.H. Lin
University of California
Civil Engineering Dept
Los Angeles, California 90024

Professor G.J. Dvorak
Dept of Civil Engr
Rensselaer Polytechnic Institute
Troy, New York 12180

Dr. R.M. Christensen
Chemistry & Matrl Sci Dept
Lawrence Livermore National Laboratory
PO Box 808
Livermore, CA 94550

Professor J.R. Rice
Division of Applied Sciences
Harvard University
Cambridge, MA 02138

Professor W.M. Sharpe
The Johns Hopkins University
Dept of Mechanics
Baltimore, MD 21218

Professor C.F. Shih
Brown University
Division of Engineering
Providence, RI 02912

Professor A. Rosakis
California Institute of Tech
Graduate Aeronautical Laboratories
Pasadena, CA 91125

Professor D. Post
VA Polytechnic & State U
Dept of Engr Science & Mechanics
Blacksburg, VA 24061

Professor W. Sachse
Cornell University
Dept of Theoretical
& Applied Mechanics
Ithaca, NY 14853

Professor G.E. Springer
Stanford University
Dept of Aeronautics & Astronautics
Stanford, CA 94305

Professor H.T. Hahn
Washington University
Center for Composites Research
St. Louis, MO 63130

Professor S.K. Datta
University of Colorado
Dept of Mechanical Engineering
Boulder, CO 80309

Dr. M.L. Williams
School of Engineering
University of Pittsburgh
Pittsburgh, PA 15261

Dr. R.M. Gallagher
VP & Dean of Faculty
Worchester Polytechnic Institute
Worchester, MA 01609

Dr. D.C. Drucker
Dept of Aerospace Eng & Mechanics
University of Florida
Tallahassee, FL 32611

Dean B.A. Boley
Dept of Civil Engineering
Northwestern University
Evanston, IL 60201

master list = ldk107
July 24, 1986

UNCLASSIFIED

SECURITY CLASSIFICATION OF THIS PAGE (When Data Entered)

REPORT DOCUMENTATION PAGE		READ INSTRUCTIONS BEFORE COMPLETING FORM
1. REPORT NUMBER UWA/DME/TR-87/58	2. GOVT ACCESSION NO.	3. RECIPIENT'S CATALOG NUMBER
4. TITLE (and Subtitle) J-estimation Procedure Based on Moire Interferometry Data		5. TYPE OF REPORT & PERIOD COVERED Technical Report 6. PERFORMING ORG. REPORT NUMBER UWA/DME/TR-85/51
7. AUTHOR(s) B.S.-J. Kang and A.S. Kobayashi		8. CONTRACT OR GRANT NUMBER(s) N00014-85-K-0187
9. PERFORMING ORGANIZATION NAME AND ADDRESS Department of Mechanical Engineering, FU-10 University of Washington Seattle, Washington 98195		10. PROGRAM ELEMENT, PROJECT, TASK AREA & WORK UNIT NUMBERS
11. CONTROLLING OFFICE NAME AND ADDRESS Office of Naval Research Arlington, VA 22217		12. REPORT DATE August 1987 13. NUMBER OF PAGES 19
14. MONITORING AGENCY NAME & ADDRESS(if different from Controlling Office)		15. SECURITY CLASS. (of this report) Unclassified 15a. DECLASSIFICATION/DOWNGRADING SCHEDULE

16. DISTRIBUTION STATEMENT (of this Report)

Unlimited

17. DISTRIBUTION STATEMENT (of the abstract entered in Block 20, if different from Report)

18. SUPPLEMENTARY NOTES

19. KEY WORDS (Continue on reverse side if necessary and identify by block number)

J-integral, moire interferometry, stable crack growth, resistance curve.

20. ABSTRACT (Continue on reverse side if necessary and identify by block number)

A j-estimation procedure based on a single displacement field obtained from moire interferometry data was developed. Accuracy assessment of the estimation procedure is made and the procedure is used to develop the J-resistance and CTOD-resistance curves for aluminum SEN specimens.

DD FORM 1 JAN 73 1473 EDITION OF 1 NOV 65 IS OBSOLETE
S/N 0102-014-6601

UNCLASSIFIED

SECURITY CLASSIFICATION OF THIS PAGE (When Data Entered)

END

DATE

FILMED

DEC.

1987